Paper:
Wang, M., Feng, Y., Zhao, T. & Wang, Y. (2019). Modelling of sand production using a mesoscopic bonded particle lattice Boltzmann method. *Engineering Computations*
http://dx.doi.org/10.1108/EC-02-2018-0093

[Modelling of sand production using a mesoscopic bonded particle lattice Boltzmann method]

Author Details:

Min Wang

Rockfield Software Limited, Swansea, Wales, SA1 8AS, UK

Y.T. Feng

Zienkiewicz Centre for Computational Engineering, Swansea University, Swansea, SA 1 8EN, UK

T.T. Zhao

Zienkiewicz Centre for Computational Engineering, Swansea University, Swansea, SA 1 8EN, UK

Yong Wang

State Key Laboratory of Geomechanics and Geotechnical Engineering, Institute of Rock and Soil Mechanics, Chinese Academy of Sciences, Wuhan, Hubei 430071, P. R. China

Corresponding author: Min Wang

Corresponding Author's Email: sacewangmin@gmail.com

Acknowledgments (if applicable):

We gratefully acknowledge the financial support from the national natural science foundations of Chin a (No. 51579237)

Structured Abstract:

Sand production is a challenging issue during hydrocarbon production in the oil and gas industry. This paper investigates one sand production process, i.e. transient sand production, using a coupled bonded particle lattice Boltzmann method. The mesoscopic fluid-particle coupling is directly approached by the immersed moving boundary method without introducing any empirical fluid-solid coupling equation. The onset of grain erosion of rocks, which are modelled by a bonded particle model, is realised by breaking the bonds simulating cementation when the tension or tangential force exceeds critical values. Prior to the simulation of transient sad production, this coupled technique is calibrated against a benchmark, i.e. flow past a cylinder. It is found that the microscopic particle erosion process can be directly captured by the proposed technique. Moreover, the simulated sand production area is consistent with experimental results.

Keywords:

Sand production; Bond model; Lattice Boltzmann method; Fluid-solid interaction; Particle erosion

Article Classification:

Research paper

For internal production use only

Running Heads: **Modelling of sand production using BPLBM**

1 Introduction

Sand production is the process of sand particles being eroded from rock formation and washed into the borehole by the reservoir fluids flow. When the rock around the wellbore undergoes plastic deformation due to stress concentrations around the cavity, the formation bond will be weakened so that the hydrodynamic force applied can dislodge sand particles from the rock formation. Then the eroded sand particles are thrust into the borehole.

Sand production is detrimental to oil and gas exploitation, it can also cause disastrous facility failures. The problems caused by sand production include: failure of the sand control completions, plugging of the perforations, borehole instability and increase in the cost of cleanup and remedial operations. It is found that 70% of the hydrocarbons in the world are located in reservoirs with poorly consolidated formations, which are susceptible to sand production due to weak bond and microstructure of formations. Therefore, understanding the mechanisms of sand production process, predicting the rate of sand production are of paramount importance in the oil and gas recovery.

To date, different methods, including the laboratory and field tests, empirical or analytical models, and numerical methods, have been developed to investigate the mechanism of sand production and predict the erosion process of sand. Cook *et al*. (1994) experimentally investigated sand production of a weakly consolidated rock using a basic cell configuration. Both axial and radial fluid flow are considered. To better represent the in-situ stress condition of reservoirs, Bianco and Halleck (2001) carried out sand production tests with a modified apparatus, through which the confining pressure can be applied to the sand sample. The set-up was a cylindrical pressure cell of 127 mm internal diameter and capable of handling pressures up to13.8 MPa. The effect of grain size on sand production was investigated by Fattahpour *et al.* (2012) through a series of laboratory experiments. It was found that for the samples with finer grain size the required confining stress for different sanding levels increased with a decrease in grain size; While, for samples with coarser grains the requested confining stress increases quickly when the grain size increases. Laboratory tests are commonly costly, complicated to operate, and time-consuming (Clearly *et al*., 1979). In addition, because the laboratory setup is small scaled, the accuracy is usually influenced by boundary treatment.

Analytical models, based on shear and tensile failure criteria (Veeken *et al*., 1991), critical plastic deformation criteria (Morita & Fuh, 1998) and erosion-based criteria (Papamichos & Malmanger, 1999), are extensively used for the investigation of sand production due to their high efficiency. However, most of those methods are only good to predict the onset of sand production, and cannot describe the movement of sand particles along with the fluid (Van den Hoek *et al*., 2000a). Combining with analytical models, the numerical methods has become most popular and powerful approaches for sand production prediction. Currently, most of numerical models used are based on the continuum approach (Morita *et al*., 1989, Vardoulakis *at al.*, 1996, Wan & Wang, 2000, Wan & Wang, 2004), in which the solid and fluid are treated as continuous in deriving the governing differential equations. Later, the convection dominated mixture theory (Vardoulakis *at al.*, 1996), including mass balance equations for solid and fluid, constitutive laws for sand erosion and Darcy flow of porous fluid, was extended for diffusion dominated flow, and Brinkman's extension of Darcy's law is adopted to account for a smooth transition between channel flow and Darcy flow (Vardoulakis *at al.*, 2001). The assumption of continuity implies that the breakage of bond connecting particles and crushing of sand particles, which are important components in sand production, are not considered. Hence, these models are hard to simulate the disaggregation and the movement of detached sand particles.

To resolve the above-mentioned problems, coupled mesoscopic techniques combining the discrete element method (DEM) and fluid solvers (computational fluid dynamics and the lattice Boltzmann method) were recently employed or developed for the modelling of sand production. Li *et al*. (2006) used a combined discrete element method-computational fluid dynamics (DEMCFD) to investigate the mechanism of sand production from the grain level. Sandstones were simulated as bonded granular media and particle erosion was obtained by bond breakage. Three different wellbore failure patterns were observed. Recently, a discrete element lattice Boltzmann method was applied for the modelling of sand production by Boutt *et al*. (2011), and successfully captured initial sand production associated with early-time drawdown. The numerical results were qualitatively consistent with laboratory and field observations. Later, Climent *et al*. (2014) carried out a 3D numerical model to simulate sand production around perforations based on the commercial software PFC where the DEMCFD was built.

The commonly encountered transient sand production is a burst of sand caused due to the reduction in the well pressure right after a perforation job in the oil industry. In this paper, a coupled bonded particle lattice Boltzmann method (BPLBM) will be employed for the investigation of transient sand production at the grain level. This approach, resolving the fluid-solid interaction by processing mesoscopic collisions of fluid particles and solid boundaries, provides an insight to the particle erosion process in sand production. The micro-mechanism of sand production will be introduced first in the next section, followed by a brief introduction of BPLBM and its validation in Section 3. Numerical evaluation of sand production is carried out and discussed in Section 4.

2 Micro-mechanism of sand production (Fjar *et al*., 2008)

Consider a sand grain of diameter d_g squeezed in between its neighbouring grains, see Fig. 1. The force needed to remove the grain is noted as F_r. It can be estimated as the sum of the shear forces, needed to induce shear failure in the four contact planes at the side of the grain, plus the force needed to induce tensile failure in the contact plane behind the grain. The hydrodynamic force (Fjar *et al*., 2008) can be given as

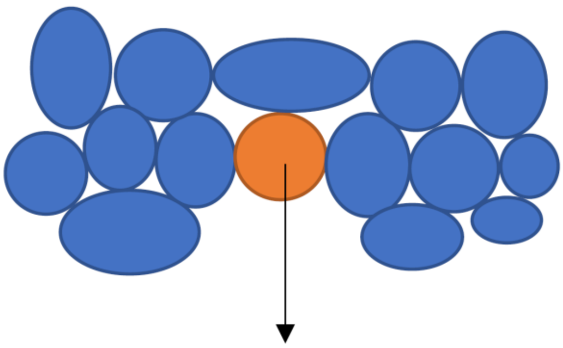

Fig 1. Sand grain at wellbore cavity

$$F_r = \pi(d_g/2)^2[4S_0 + \mu(2\sigma_z^{'} + \sigma_\theta^{'}) + T_0] \quad (1)$$

where T_0 and S_0 are the tensile strength and the cohesion, respectively; μ is the coefficient of internal friction; and $\sigma_z^{'}$ and $\sigma_\theta^{'}$ are the effective axial and tangential stresses, respectively, at the cavity wall.

The hydrodynamic forces applied to the grain are caused by the flowing of pore fluid. An estimate of the forces can be obtained as follows: The force F acting on a volume element of the rock due to a fluid flowing through it is

$$F = -A\Delta P_f \quad (2)$$

where A is the cross-sectional area through which the fluid is flowing, and ΔP_f is the pore pressure drop over the length of the volume element Δx.

Then the average hydrodynamic force F_h acting on one grain within the volume element is

$$F_h = F/N = -A\Delta P_f/N \tag{3}$$

where N is the total number of grains in the volume element.

3 Numerical methods

In BPLBM, the solid material is treated as an assembly of bonded particles and the macroscopic behaviour of the solid is the comprehensive reflection of the inter-particle interactions. The bond model is utilised to handle the cohesive forces between bonded particles, and the treatment of the contact between granular particles are the same as that in DEM. Moreover, the fluid flow is solved using the lattice Boltzmann method and the fluid-solid interactions are achieved through the immersed moving boundary (IMB) scheme (Noble and Torczynski, 1998). For the sake of consistency, a brief description of the bonded particle model (BPM), together with LBM and IMB, will be given in this section. A detailed introduction of these methods can be found in the references (Wang *et al*., 2016, Wang *et al*., 2017a,b).

3.1 Bonded particle method

Two issues need to be carefully resolved in BPM. One is the movement of solid particles, and the other is the treatment of particle contact.

The motion of a particle is governed by Newton's second law

$$ma + cv = F_c + F_f + mg \tag{4}$$

$$I\ddot{\theta} = T_c + T_f \tag{5}$$

where m and I are respectively the mass and the moment of inertia of the particle; *c* is a damping coefficient; a and $\ddot{\theta}$ are the acceleration and angular acceleration respectively; F_c and T_c are, respectively, contact forces and the corresponding torques, F_f and T_f are the hydrodynamic forces and the corresponding torques.

In BPM, there are two interactions between solid particles: the particle-particle contact existing between granular particles and the cohesion between bonded particles. As the treatment of particle-particle interactions is the same as that in DEM (Wang *et al*., 2016), only the treatment of cohesion, which is simulated by bond models, will be given in this section.

3.1.1 Bond model

It has been well understood that the bonds existing between adjacent particles can resist both traction and shear forces. It will break due to excessive traction and/or shear forces (Delenne *et al*., 2004, Jiang *et al*., 2012). The bonded model adopted in this work is proposed by Wang *et al*. (2017b) based on the experimental data (Delenne *et al*., 2004, Jiang *et al*., 2012). It includes a normal bond considering the softening effect and a history dependent Coulomb friction model. Its normal force F_n^b and tangential force F_t^b are given by

$$F_n^b = \begin{cases} K_n^b \delta & \delta >= \delta_1 \\ K_n^b \delta_1 + K_{sf}(\delta - \delta_1) & \delta_2 < \delta < \delta_1 \\ 0 & \delta < \delta_2 \end{cases} \tag{6}$$

$$F_t^b = -\frac{\dot{\delta}_t}{\left|\dot{\delta}_t\right|} \begin{cases} K_t^b \left|\delta_t\right|; & \left|K_t^b \delta_t\right| \le \mu F_n^b \\ \mu F_n^b; & \left|K_t^b \delta_t\right| > \mu F_n^b \end{cases} \tag{7}$$

where K_n^b and K_t^b are the normal stiffness and tangential stiffness for the cement; F_{bn} is the critical tensile force and F_{bt} is critical shear strength; K_{sf} , δ_1 and δ_2 are, respectively, the stiffness for the softening period, the overlap corresponding to the critical bond force and the overlap corresponding to the bond breakage; and μ is the coefficient of friction.

3.2 Lattice Boltzmann method

The lattice Boltzmann method is a kind of modern computational fluid dynamics. Compared to the conventional CFD and the lattice gas automata based on movement of microscopic cells, LBM is can be treated as a mesoscopic computational method. It is upscaled from the lattice gas automata through statistical law of fluid particles. The fluid domain is divided into regular lattices. The fluid phase is treated as a group of (imaginary) fluid particle packages which carry mass and momentum. Each particle package includes several particles which are allowed to move to the adjacent lattice nodes or stay at rest. The flow of fluid can be achieved through resolving particle collision and streaming processes governed by the lattice Boltzmann equation. Unlike the conventional CFD where pressure, velocity and density are primary variables, the primary variables of LBM are the so-called fluid density distribution functions for each fluid particle package at the lattice nodes.

The lattice Boltzmann equation is described by

$$f_i(x + e_i \Delta t, t + \Delta t) - f_i(x, t) = \Omega_i \tag{8}$$

where f_i are the fluid density distribution functions; x and e_i are the coordinate and velocity vectors at the current lattice node; t and Ω_i are, respectively, the current time and the collision operator.

In the single relaxation Lattice BGK Model (Qian et al., 1992), Ω_i is characterised by a relaxation time τ and the equilibrium distribution functions $f_i^{eq}(x, t)$.

$$\Omega_i = -\frac{\Delta t}{\tau}\left[f_i(x, t) - f_i^{eq}(x, t)\right] \tag{9}$$

In this work, the D2Q9 model (Succi, 2001) in Lattice BGK is adopted. The macroscopic fluid density ρ and velocity v can be calculated from the distribution functions

$$\rho = \sum_{i=0}^{8} f_i, \qquad \rho v = \sum_{i=1}^{8} f_i e_i \tag{10}$$

The fluid pressure is given by

$$P = C_S^2 \rho \tag{11}$$

where C_S is termed the fluid speed of sound, defined as $C_S = h/(\sqrt{3}\Delta t)$. h is lattice spacing and Δt is time step.

For more details of the fundamental of LBM, the reference (Tran et al., 2017) is recommended.

3.3 Fluid-particle coupling

The immersed moving boundary scheme was proposed by Noble and Torczynski (1998) to overcome fluctuations of hydrodynamic forces calculated through smoothly representing the boundaries of solid particles when they are moving. In this method, the particle is represented by solid nodes, the solid boundary nodes and interior solid nodes. The fluid nodes near the solid boundary nodes are defined as the fluid boundary nodes. A schematic diagram of IMB is shown in Fig. 2. Four sets of nodes: solid boundary nodes, interior solid nodes, fluid boundary nodes and normal fluid nodes, are marked in red, yellow, green and blue, respectively. In order to retain the advantages of LBM, namely the locality of the collision operator and the simple linear streaming operator, an additional collision term, Ω_i^S, for nodes covered partially or fully by the solid is introduced to the standard collision operator of LBM.

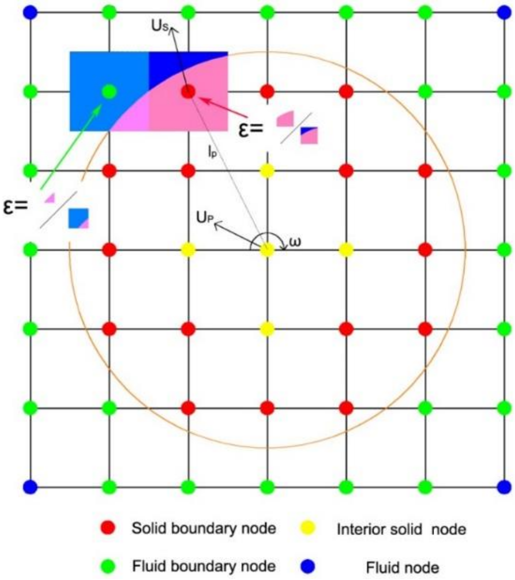

Fig. 2 IMB scheme and definition of local solid ratio ε (after Wang *et al*., 2017a)

The modified collision operator for resolving the fluid-solid interaction is given by

$$\Omega_i = -\frac{\Delta t}{\tau}(1 - B)[f_i(x, t) - f_i^{eq}(x, t)] + B\Omega_i^S \tag{12}$$

where *B* is a weighting function that depends on the local solid ratio ε, defined as the fraction of the node area (see Fig. 2):

$$B = \frac{\varepsilon(\tau - 0.5)}{(1-\varepsilon)+(\tau - 0.5)}$$

The added collision term (Ω_i^S) is based on the bounce-rule for nonequilibrium part and is given by

$$\Omega_i^S = f_{-i}(x, t) - f_i(x, t) + f_i^{eq}(\rho, U_S) - f_{-i}^{eq}(\rho, u) \quad (13)$$

where U_S is the velocity of the solid node (see Fig. 2) and u is the fluid velocity of each node.

The resultant hydrodynamic force F_f and torque T_f exerted on the solid particle can be calculated from momentum theorem.

3.4 Validation of fluid-solid interaction

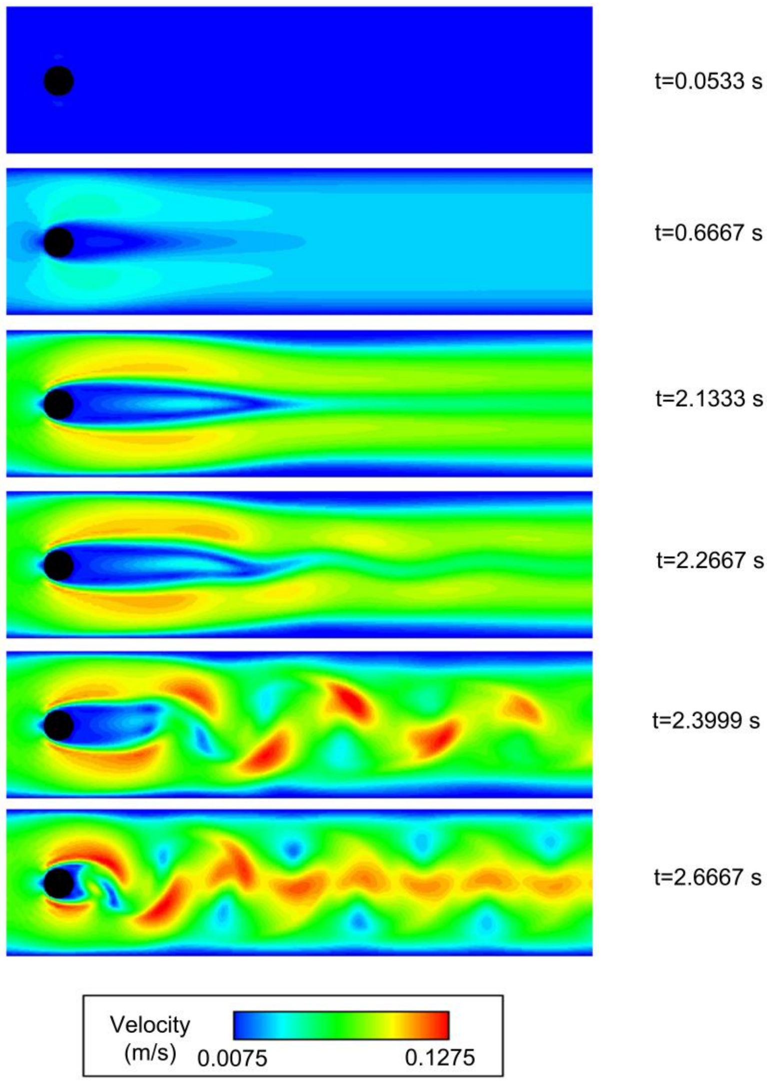

Fig. 3 Flow passing a cylinder: Velocity contours at different time instants

A benchmark test, flow passing a cylinder, is carried out to validate the IMB scheme. This example concerns steady and unsteady flows around a circular cylinder placed in a long rectangular channel. The channel (see Fig. 3) is 1 cm in height (the *Y* direction) and 8 cm in length (the *X* direction). A cylinder of 0.2 cm in diameter is placed at the position (2.0, 0.5) cm. Both top and bottom boundaries are stationary walls where the no-slip boundary condition is applied. The pressure boundary condition is applied on the left boundary and the right boundary with a pressure difference of 7.5 kPa. The lattice spacing of 0.01 cm is chosen so that the fluid domain is divided into 800×100 lattices. The relaxation parameter τ is 0.5001.

The velocity contours at different time instants are shown in Fig. 3. It is observed that when the fluid approaches the front side of the cylinder, the fluid pressure increases and the fluid is forced to move around the cylinder surface. When the Reynolds number exceeds a threshold, the fluid cannot follow the cylinder surface to the rear side but separates from both sides, and a pair of symmetric vortices are formed in the near wake (t = 0.6667 s). As the Reynolds number (*Re*>45) further increases, the wake becomes unstable. One vortex will draw the opposite vortex across the wake, and then vortex shedding is initiated at t = 2.2667 s where the Reynolds number further increases to about 100.

The quantitative comparison of the drag coefficient C_d calculated using LBM against the experimental, theoretical and CFD numerical results (Sato & Kobayashi, 2012) is presented in Fig. 4. It is found that the drag coefficients for Reynolds numbers (*Re*) between 10 and 110 match the experimental and CFD data very well; while there are certain differences when *Re* is lower than 10. Interestingly, for the Stokes flow (*Re*<1) the proposed LBM procedure is much closer to the theoretical result described by Eq. 14.

$$C_d = \frac{24}{Re} \tag{14}$$

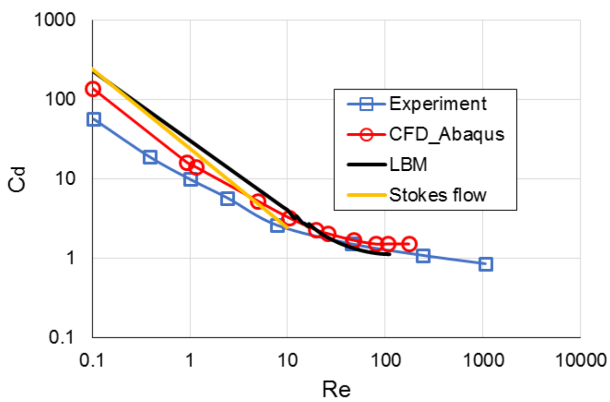

Fig. 4 Comparison of drag coefficient vs Reynolds number

4 Numerical simulation and discussions

A 2D wellbore model, with dimensions $1\,m \times 1\,m$, is considered in this work, as shown in Fig. 5. To reduce the computational cost, half of the axisymmetric model including 3591 particles will be simulated. The radii of grains range from 6 to 10 mm. The friction coefficient of 0.1, and the normal and tangential stiffness of 5.0×10^7 *N/m* are set to all particles. The sandstone sample with an initial cavity radius of 0.22 m is first generated with a desired initial stress 30 Mpa. When the mechanical balance is obtained, the radius of the mechanical constraint at the cavity is gradually reduced. Finally, the cavity constraint is removed to re-obtain a balanced state.

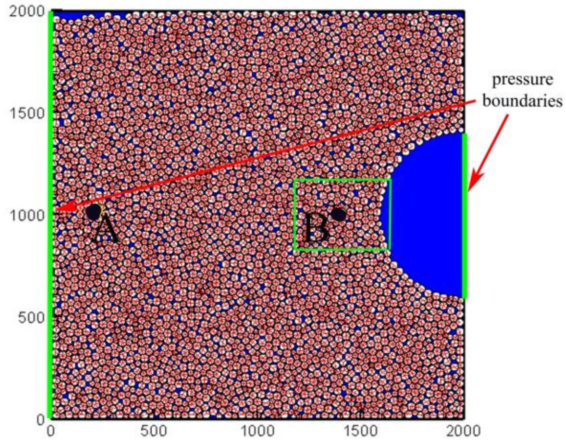

Fig. 5 Wellbore model

It has been reported that to achieve an accurate solution the diameter of the smallest particle should cover at least 10 fluid grids (Wang *at al*., 2017a). The fluid domain is divided into 2000×2000 lattices with grid spacing $h = 0.5\ mm$. The ratio of the smallest diameter to the grid spacing adopted in this paper is 24 which can ensure the accuracy of simulation. The time step used in this simulation is $8.333\times10^{-7}\ s$. Other parameters of the fluid and bond models are listed in Table 1. In the fluid model, two pressure boundaries marked in green are applied to both the left boundary and the middle segment of the right boundary. The right pressure is lower than the left one. The pressure difference between the left and right boundaries is stepwise increased to 100 kPa and given in Fig.6. For ease of implementation, other fluid boundary conditions are applied no-slip bounce back.

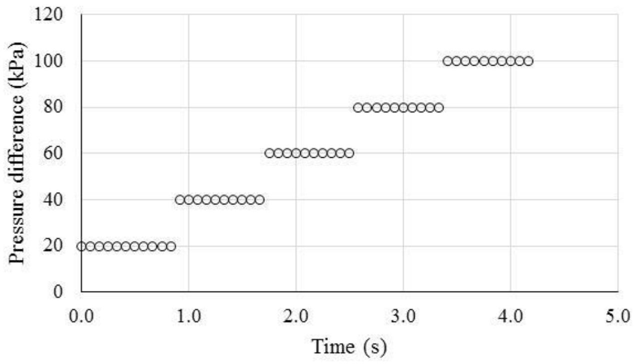

Fig. 6 Pressure difference applied

Table 1 Parameters for the fluid and solid

Parameter	Value	Parameter	Value
Particle density (kg/m^3)	3000	Fluid density (kg/m^3)	1000
Critical bond force (N)	5	Bond contact stiffness (N/m)	2.0×10^{7}
Contact damping ratio (ξ)	0.5	kinematic viscosity (υ)	1.0×10^{-6}

In the 2-D simulation by combining DEM and other fluid methods, such as CFD and LBM, there is a major issue in the pore water flow path. Because the flow paths are always blocked up by contacted particles, it is difficult to obtain realistic flow channels. In order to solve this problem, Boutt *et al*. (2007) proposed a method in which the radius of a particle will be artificially reduced to a certain degree (called the effective radius) when the fluid flow is implemented. This effective hydraulic radius can be accomplished by introducing a ratio of the effective radius to the particle radius. In this work, the ratio of 0.85 is adopted.

Transient sand production is commonly observed after a perforation job. This post perforation process is simulated by the removal of the cavity constraint mentioned above. Then, the drawdown of fluid pressure is applied to the wellbore cavity. The fluid velocity contours, the deformation of sandstone and grain distribution when balance status is reached under each leading are shown in Fig. 7. As there is no particle erosion but only finite solid deformation under the first-level loading, only the snapshots from the second-level fluid loading (40 kPa) are given here.

During the whole simulation, the Mach number Ma is calculated by

$$Ma = \frac{U}{C} \tag{15}$$

where U is the fluid velocity in lattice unit, and $C = \sqrt{3}C_s$ is the lattice speed. The Mach number is much smaller than 1. Hence an incompressible fluid flow can be guaranteed.

The computed Reynolds number for the pore fluid flow is 104. It is within the range validated in aforementioned flow passing a cylinder.

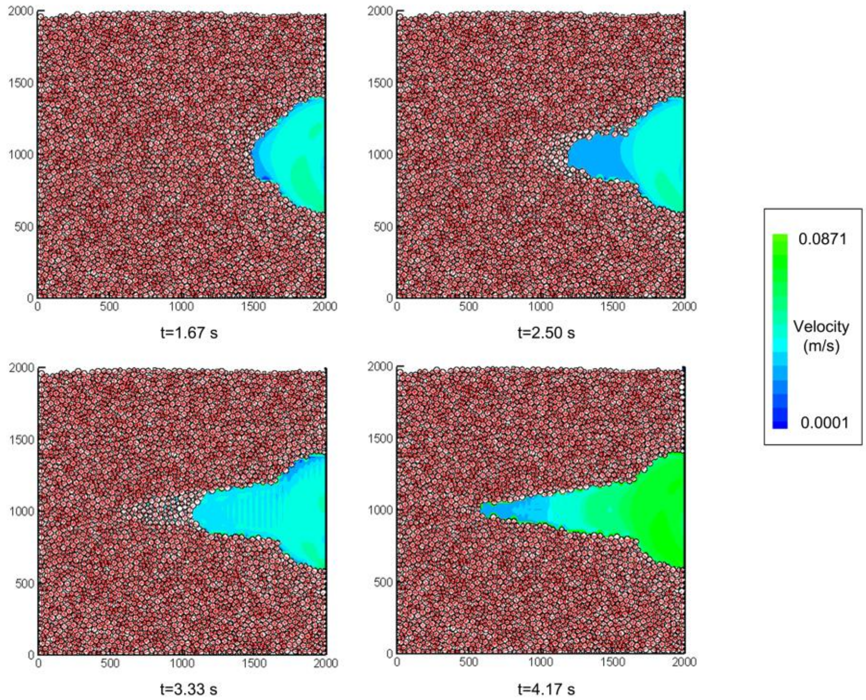

Fig. 7 Sand production process

In this simulation, the bond failure process is governed by the tensile strength. When the tensile strength exceeds 5 N, the bond existing between particles marked in red will be removed. From Fig. 7 it can be found that some grains are first eroded along the middle line of wellbore cavity under the pressure difference 40 kPa. With the increase of pressure difference, fluid velocity increases and the tensile failure area gradually propagates inward. Then, more and more particles in the formation are eroded.

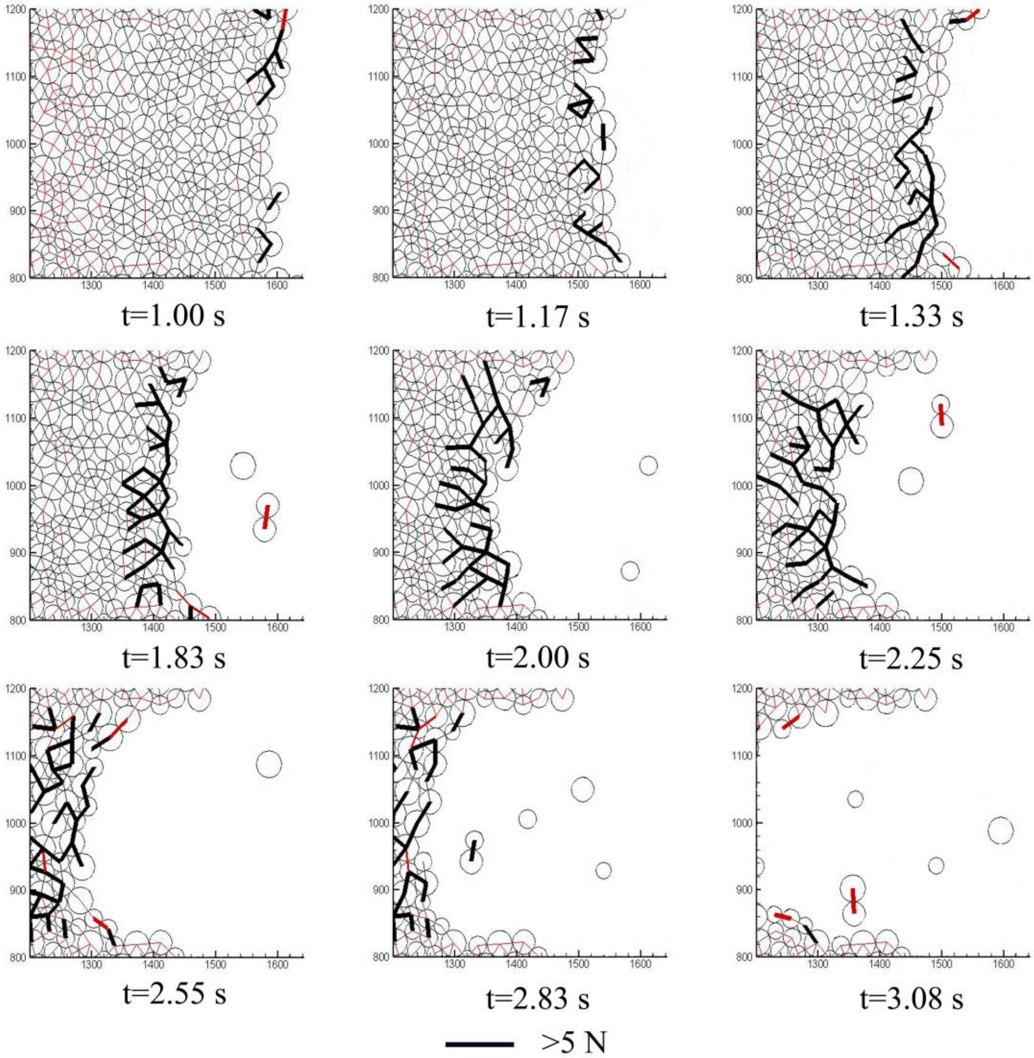

Fig. 8 Bond distribution and force chain at different instants

To better understand the erosion process, a local part around the wellbore cavity enclosed by green box in Fig. 5 is zoomed in and the snapshot of this region at different instants are given in Figure. 8 where lines connecting particle centres represent the bond. The red and black colours represent the compression and tension status of the bond. The width of the bond indicates the magnitude of force. The tensile and compressive forces larger than the bond strength 5 N are plotted in bold lines. These bold lines represent the oncoming bond failure. It can be seen from Fig. 8 the bond breakage propagates inward with time, and the solid particles at the tensile failure area become eroded due to large drag forces which exceed the sum of shear and cohesion forces applied by surrounding particles. Subsequently, some eroded particles are washed out. The erosion process of particles continues with time and increasing loadings.

To validate the simulation of sand production, the experimental results of sanding area carried out by van den Hoek *et al*. (2000b) is chosen for comparison. Due to the limitation of experimental techniques, the transient sanding process is hard to be captured. Hence only the final shape of the sanding area is shown in Fig. 9. It can be found that the geometry of the sanding area in our simulation is consistent with the experimental observation.

Fig. 9 Experimental results of sand production

Figs. 10 and 11 show the evolution of the fluid velocity at position A and B shown in Fig. 5. It is seen that the fluid velocity increases quickly till reaching balance under each fluid pressure difference. With the increase of pressure drawdown, the fluid velocity at both positions increases. It is noticed that the fluid velocity at position B abruptly increases around 2.0 s. This phenomenon is caused by the particle erosion process. It can be seen from Fig. 8, particles at position B are eroded during this time period. Then large velocity difference is caused at the interface between rock formation and fluid outside. It furthers the erosion of particles at the interface.

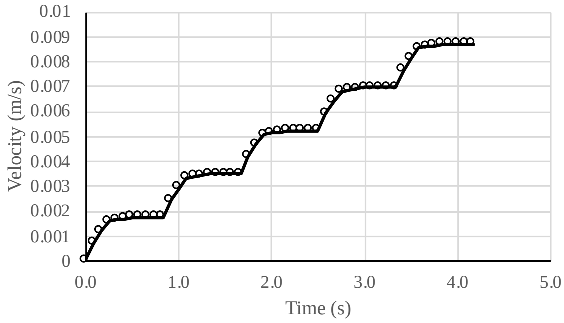

Fig. 10 Variation of fluid velocity at position A

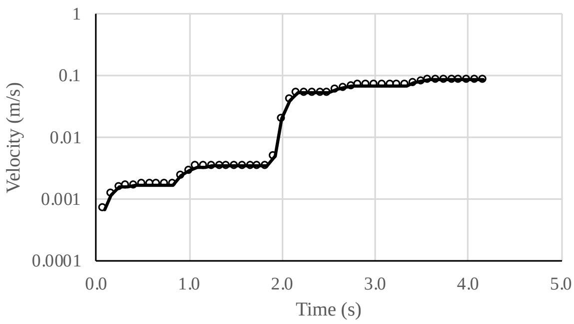

Fig. 11 Variation of fluid velocity at position B

Challenging problems in sand production modelling include the mesoscopic fluid-particle interactions and the particle breakage of large-sized aggregates. This paper mainly focuses on the treatment of the mesoscopic fluid-particle interaction at the grain level. Based on the bond model applied between bonded particles, the transient particle erosion process can be captured. The subsequent movement of eroded sand grains are successfully simulated. Here, sand particles moved into the wellbore cavity by fluid are treated as eroded particles. Then, the erosion ratio $R_{erosion}$ of the formation can be computed by Eq. 16,

$$\mathrm{R}_{\mathrm{erosion}} = \frac{\mathrm{Mass}_{\mathrm{erosion}}}{\mathrm{Mass}_{\mathrm{formation}}} \tag{16}$$

where $Mass_{erosion}$ is the mass of eroded particles; $Mass_{formation}$ is the original mass of formation sand particles.

Fig. 12 displays the evolution of the erosion ratio of formation sand. It can be observed that at the earlier stage of simulations no eroded particles can be detected when pressure difference is as low as 20 kPa. Erosion of particles starts at the second stage when the pressure difference is increased to 40 kPa. At this stage particle erosion ratio increase quickly first. Then the erosion rate decrease with time at each loading stage till the erosion ratio reaches balance. When the fluid pressure difference is increased to 60 kPa, significant increase of erosion ratio is observed.

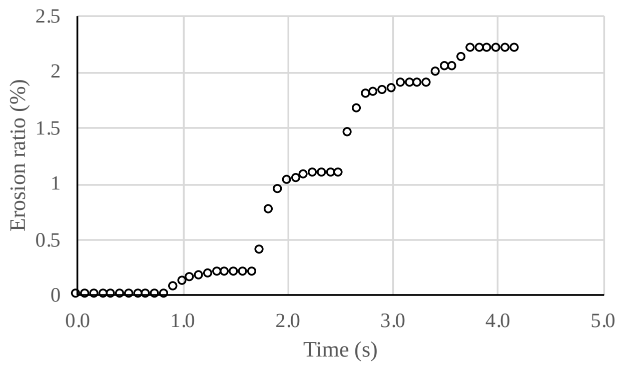

Fig. 12 Evolution of erosion ratio of formation

In the existing research using continuum-based methods, the transient particle transport, which plays an important role in continuous sand production, is overlooked. Therefore, this proposed BPLBM bridges the gap between the underlying physics of micro-mechanical interactions of fluid and solid grains and the continuum descriptions of those systems.

The two-dimensional simulation in this research is carried out using a desktop computer (Intel Core i5-3450 CPU@3.10GHz), and takes about 111 hours 14 minutes. The computing cost depends on the number of solid particles and the grid size of LBM. The high ratio of the smallest radius to the grid spacing could achieve a better simulation accuracy. Meanwhile, it will inevitably cause much more computing time. Field observation indicates that the transient sand production is mainly caused by hydraulic loading. In the continuous sand production process, the particle breakage of large-sized aggregates to fine grains needs to be considered. The proposed BPLBM cannot simulate particle breakage problems at the present stage. Further work on the bond model will be undertaken to resolve this issue in the near future.

5 Conclusions

In this paper, a sand production model has been simulated by a recently proposed bonded particle lattice Boltzmann method. The accuracy of this coupled method is examined by an extensively investigated benchmark test. It is proved that the complex fluid-solid interaction occurring at the pore/grain level can be well captured by the immersed moving boundary scheme in the framework of the lattice Boltzmann method. It is found that when the drawdown happens at the wellbore cavity, the tensile failure area appears at the edge of the cavity. Then, the tensile failure area gradually propagates inward, and the solid particles at the tensile failure area become eroded due to large drag forces. Subsequently, some eroded particles are washed out. This numerical investigation is demonstrated through comparison with the experimental results. In addition, through breaking the cementation, which is simulated by bond models, between bonded particles, the transient particle erosion process is successfully captured. The subsequent movement of eroded sand grains can also be well simulated. However, the computational cost of this completely particle-based coupling method is inevitably expensive.

References

Bianco, L. C. B., & Halleck, P. M. (2001). Mechanisms of arch instability and sand production in two-phase saturated poorly consolidated sandstones. In *SPE European Formation Damage Conference*. Society of Petroleum Engineers.

Boutt DF, Cook BK, McPherson BJOL, Williams JR. Direct simulation of fluidsolid mechanics in porous media using the discrete element and lattice-Boltzmann methods. J Geophys Res 2007;112:B10209.

Boutt, D. F., Cook, B. K., & Williams, J. R. (2011). A coupled fluid–solid model for problems in geomechanics: application to sand production. *International Journal for Numerical and Analytical Methods in Geomechanics*, *35*(9), 997-1018.

Clearly, M. P., Melvan, J. J., & Kohlhaas, C. A. (1979). The effect of confining stress and fluid properties on arch stability in unconsolidated sands. In *SPE Annual Technical Conference and Exhibition*. Society of Petroleum Engineers.

Climent, N., Arroyo, M., O'Sullivan, C., & Gens, A. (2014). Sand production simulation coupling DEM with CFD. *European Journal of Environmental and Civil Engineering*, *18*(9), 983-1008.

Cook, J. M., Bradford, I. D. R., & Plumb, R. A. (1994). A study of the physical mechanisms of sanding and application to sand production prediction. In *European Petroleum Conference*. Society of Petroleum Engineers.

Delenne, J.-Y., El Youssoufi, M. S., Cherblanc, F. & Bénet, J.-C. 2004. Mechanical behaviour and failure of cohesive granular materials. *International Journal for Numerical and Analytical Methods in Geomechanics*, 28, 1577-1594.

Fjar, E., Holt, R. M., Raaen, A. M., Risnes, R., & Horsrud, P. (2008). *Petroleum related rock mechanics*. Elsevier, Amsterdam, Netherlands.

Fattahpour, V., Moosavi, M., & Mehranpour, M. (2012). An experimental investigation on the effect of grain size on oil-well sand production. *Petroleum Science*, *9*(3), 343-353.

Jiang, M. J., Sun, Y. G., Li, L. Q. & Zhu, H. H. 2012. Contact behavior of idealized granules bonded in two different interparticle distances: An experimental investigation. *Mechanics of Materials*, 55: 1-15.

Li, L., Papamichos, E., & Cerasi, P. (2006). Investigation of sand production mechanisms using DEM with fluid flow. *Multiphysics Coupling and Long Term Behaviour in Rock Mechanics*, 241-247.

Morita, N., Whitfill, D. L., Massie, I., & Knudsen, T. W. (1989). Realistic sand-production prediction: numerical approach. *SPE Production Engineering*, *4*(01), 15-24.

Morita, N., & Fuh, G. F. (1998). Prediction of sand problems of a horizontal well from sand production histories of perforated cased wells. In *SPE Annual Technical Conference and Exhibition*. Society of Petroleum Engineers.

Noble, D. R., & Torczynski, J. R. (1998). A lattice-Boltzmann method for partially saturated computational cells. *International Journal of Modern Physics C*, *9*(08), 1189-1201.

Papamichos, E., & Malmanger, E. M. (1999). A sand erosion model for volumetric sand predictions in a North Sea reservoir. In *Latin American and Caribbean Petroleum Engineering Conference*. Society of Petroleum Engineers.

Qian, Y. H., D'humières, D. & Lallemand, P. 1992. Lattice BGK Models for Navier-Stokes Equation. *Europhysics Letters*, 17, 479-484.

Sato, M., & Kobayashi, T. (2012). A fundamental study of the flow past a circular cylinder using Abaqus/CFD. In *2012 SIMULIA Community Conference*.

Succi, S. 2001. The Lattice Boltzmann Equation for Fluid Dynamics and Beyond. Oxford University Press.

Tran, D.K., Prime, N., Froiio, F., Callari, C. and Vincens, E., (2017) Numerical modelling of backward front propagation in piping erosion by DEM-LBM coupling. *European Journal of Environmental and Civil Engineering*, 21(7-8), pp.960-987.

Van den Hoek, P. J., Hertogh, G. M. M., Kooijman, A. P., De Bree, P., Kenter, C. J., & Papamichos, E. (2000a). A new concept of sand production prediction: theory and laboratory experiments. *SPE Drilling & Completion*, *15*(04), 261-273.

Van den Hoek, P. J., Kooijman, A. P., De Bree, P., Kenter, C. J., Sellmeyer, H. J., & Willson, S. M. (2000b). Mechanisms of downhole sand cavity re-stabilisation in weakly consolidated sandstones. In *SPE European Petroleum Conference*. Society of Petroleum Engineers.

Vardoulakis, I., Stavropoulou, M., & Papanastasiou, P. (1996). Hydro-mechanical aspects of the sand production problem. *Transport in porous media*, 22(2), 225-244.

Vardoulakis, I., Papanastasiou, P., & Stavropoulou, M. (2001). Sand erosion in axial flow conditions. *Transport in Porous Media*, 45(2), 267-280.

Veeken, C. A. M., Davies, D. R., Kenter, C. J., & Kooijman, A. P. (1991). Sand production prediction review: developing an integrated approach. In *SPE annual technical conference and exhibition*. Society of Petroleum Engineers.

Wan, R. G., & Wang, J. (2000). Modelling sand production within a continuum mechanics framework. In *Canadian International Petroleum Conference*. Petroleum Society of Canada.

Wan, R. G., & Wang, J. (2004). Modelling of sand production and wormhole propagation in an oil saturated sand pack using stabilized finite element methods. *Journal of Canadian Petroleum Technology*, *43*(04).

Wang, M., Feng, Y.T. & Wang, C.Y. (2016) Coupled bonded particle and lattice Boltzmann method for modelling fluid–solid interaction, *International Journal of Numerical and Analytical Methods in Geomechanics*, 40: 1383-1401.

Wang, M., Feng, Y.T. & Wang, C.Y. (2017a) Numerical investigation of initiation and propagation of hydraulic fracture using the coupled Bonded Particle–Lattice Boltzmann Method, *Computers & Structures*, 181: 32-40.

Wang, M., Feng, Y.T., Pande, G.N. et al., (2017b) Numerical modelling of fluid-induced soil erosion in granular filters using a coupled bonded particle lattice Boltzmann method, *Computers and Geotechnics*, 82: 134-143.

Figures list

Fig 1. Sand grain at wellbore cavity

Fig. 2 IMB scheme and definition of local solid ratio ε (after Wang *et al*., 2017a)

Fig. 3 Flow passing a cylinder: Velocity contours at different time instants

Fig. 4 Comparison of drag coefficient vs Reynolds number

Fig. 5 Wellbore model

Fig. 6 Pressure difference applied

Fig. 7 Sand production process

Fig. 8 Bond distribution and force chain at different instants

Fig. 9 Experimental results of sand production

Fig. 10 Variation of fluid velocity at position A

Fig. 11 Variation of fluid velocity at position B

Fig. 12 Evolution of erosion ratio of formation